Chimeras of Cell-Penetrating Peptides Demonstrate Synergistic Improvement in Antisense Efficacy

Chimeras of Cell-Penetrating Peptides Demonstrate Synergistic Improvement in Antisense Efficacy

Colin M. Fadzen,[†[a]] Rebecca L. Holden,[†[a]] Justin M. Wolfe,[†[a]] Zi-Ning Choo,[[a]] Carly Schissel,[[a]] Monica Yao,[[c]] Gunnar J. Hanson,[[c]] and Bradley L. Pentelute[[a,b]]*

[a] Department of Chemistry, Massachusetts Institute of Technology, Cambridge, MA 02139

[b] Extramural Member, Koch Institute MIT; Associate Member, Broad Institute of Harvard and MIT; Member, Center for Environmental Health Sciences MIT; Cambridge, MA 02139

[c] Research Chemistry, Sarepta Therapeutics, Inc., Cambridge, MA 02142

† These authors contributed equally to this work

* Corresponding author. E-mail: blp@mit.edu

ABSTRACT

Phosphorodiamidate morpholino oligonucleotides (PMOs) are a promising class of therapeutics for genetic disease. PMOs designed for "exon skipping" must be internalized into cells, reach the nucleus, and act on pre-mRNA to mediate their effects. One tactic for improving PMO delivery and exon skipping is to covalently conjugate PMOs to cell-penetrating peptides (CPPs). Here we report the synthesis of PMOs conjugated to CPP chimeras, constructed by combining multiple CPPs into one sequence. The chimeric CPPs synergistically improve PMO activity up to 70-fold over the PMO alone, beyond the expected effects of each component peptide. By investigating the design space of CPP chimeras, we demonstrate that all components must be covalently attached, that the order of the two sequences matters, and that peptide identity can tune activity. We identified one chimera (pVEC-Bpep) to investigate in more detail and found that it engages different mechanisms of endocytosis than its parent peptides. We also examined the extent to which the beneficial effect comes from improved cellular uptake as opposed to the downstream steps required for exon skipping. Given the complexity of intracellular delivery, we anticipate this work will lead researchers to consider combining molecules with different physicochemical properties in order to aid in the delivery of biologic cargoes.

TOC Graphic, For Table of Contents Use Only:

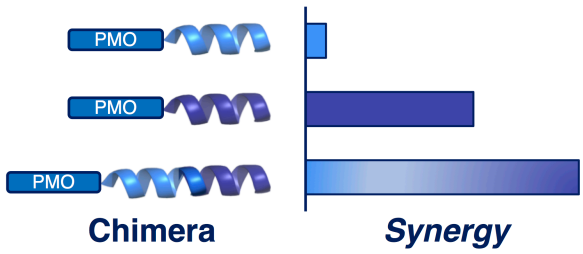

Introduction:

Phosphorodiamidate morpholino oligonucleotides (PMOs) are attractive therapeutic molecules for genetic diseases. Designed to recognize targets by Watson-Crick base pairing, PMOs exhibit a high level of specificity for their complementary nucleotide sequence. Depending on the type of sequence targeted, PMOs can mediate a variety of effects, including blocking protein translation or modifying pre-mRNA splicing. Eteplirsen, a PMO conditionally approved by the FDA to treat Duchenne muscular dystrophy, alters the splicing of the dystrophin pre-mRNA in order to restore the functionality of the dystrophin protein.[1]

In terms of structure, PMOs are neutral oligonucleotide analogues in which the ribosyl ring has been replaced with a morpholino ring and the negatively-charged phosphodiester backbone has been replaced with the uncharged phosphorodiamidate.[2] The altered backbone structure prevents degradation both in serum and by intracellular nucleases.[3,4] Yet the relatively large size and neutral charge of PMOs can lead to inefficient delivery to the cytosol and nucleus.[5]

Cell-penetrating peptides (CPPs) are a promising strategy to improve the delivery of PMO to the nucleus.[6–11] CPPs are relatively short sequences of 5-40 amino acids that ideally access the cytosol and can promote the intracellular delivery of cargo.[12,13] CPPs can be classified into different groups based on their physicochemical properties. One common CPP class consists of repetitive, arginine-based peptides such as R_{12} and Bpep (RXRRβRRXRRβR, in which X is aminohexanoic acid and β is β-alanine). These oligoarginine peptides are often random coils.[14] When conjugated to PMO, the oligoarginine peptides have been among the most effective peptides in promoting PMO delivery.[7–9] Other CPPs, such as Penetratin, pVEC, and melittin, are more amphipathic in nature. While these sequences do contain cationic residues, the defined

separation of charged and hydrophobic residues can promote amphipathic helix formation. However, amphipathic CPPs have not been demonstrated to significantly improve PMO efficacy.

No universal mechanism of cell entry exists for CPPs or CPP-PMO conjugates.[15,16] The mechanism is often highly dependent on the treatment concentrations and the type of cargo attached.[17,18] Above a certain threshold concentration (generally low micromolar), energy-independent cytosolic uptake can be observed faster than the time scale of endocytosis and cell surface recycling.[17,19] The fast uptake rate provides evidence for a direct translocation mechanism similar to what is observed for a small molecule. However, at low, physiologically-relevant concentrations, uptake is primarily endocytic. Even within the category of endocytosis, CPPs and CPP-PMO conjugates can enter cells using one or multiple endocytic mechanisms.[16,20] These endocytic mechanisms include macropinocytosis, clathrin-mediated endocytosis, caveolae-mediated endocytosis and clathrin/caveloae-independent endocytosis.[21] CPP-PMO conjugates are primarily endocytosed at low concentrations, and the CPPs that are poor for PMO delivery are likely trapped in endosomes or excluded from the nuclear compartment.

Given that different CPPs can engage different endocytic mechanisms and that some CPPs are better at escaping endosomes than others, each individual CPP has strengths and weaknesses. One way to harness the benefits of various peptides is to combine them into chimeric peptides and leverage the strengths of each component. Yin and coworkers created covalent chimeras between a muscle targeting peptide and Bpep to combine muscle targeting with cell-penetration for PMO delivery.[22] Abes *et al*. utilized one chimera composed of penetratin and a polyarginine peptide to improve the delivery of peptide nucleic acids, a different class of antisense oligonucleotide.[23] However, there has yet to be an extensive examination of the design space of

chimeras composed of two CPPs. A thorough understanding of this space is necessary in order to apply these hybrid molecules to improve PMO delivery.

To begin our investigations, we envisioned that chimeric peptides composed of a random-coil, oligoarginine CPP with an amphipathic CPP could improve PMO activity. If each CPP utilizes distinct mechanisms of endocytosis, the chimera may be able to access multiple mechanisms of cellular entry. Further, the different CPPs may have beneficial effects on processes downstream of uptake, such as endosomal escape or nuclear entry. Here, we present several amphipathic/oligoarginine CPP chimeras that exhibit a synergistic, rather than additive, gain in PMO efficacy in a biological assay. The CPP chimeras increase PMO activity in this assay up to 70-fold over the PMO alone and outperform the potent CPP standard (Bpep). We investigate several of the design principles for the success of these conjugates and probe the mechanism of uptake for one particular conjugate.

Materials and Methods:

Peptide synthesis: Peptides were synthesized on an automated flow peptide synthesizer as previously described.[24] For detailed methods on peptide synthesis and purification, please see the Supplementary Information.

PMO Azide Synthesis:

PMO IVS2-654 was provided by Sarepta Therapeutics. To conjugate the azide to the 3' end, PMO IVS2-654 was dissolved in DMSO (53 mM). To the solution was added 4 equivalents of 5-azidopentanoic acid activated with HBTU and 4 equivalents of DIEA dissolved in DMF. The reaction proceeded for 25 minutes before being quenched with water and ammonium hydroxide. The ammonium hydroxide was used to hydrolyze any ester formed during the course of the

reaction. After 1 hour, the solution was diluted and purified by reversed-phase HPLC using a linear gradient from 2% to 60% B over 58 minutes. Mobile phase A: water. Mobile phase B: acetonitrile. For LC-MS characterization, please see Supplementary Information.

Fluorophore Conjugation:

For fluorophore-labeled PMO-peptide conjugates, the organic dye was attached prior to conjugation to PMO. Equimolar SulfoCy5-maleimide was conjugated to cysteine-containing peptides in 1 mL of H_2O. After 30 minutes, the reactions were purified by reversed-phase HPLC using a linear gradient from 5-45% B over 80 minutes for pVEC and pVEC-Bpep and a linear gradient from 1-31% B over 60 minutes for Bpep. Mobile phase A: water with 0.1% TFA. Mobile phase B: acetonitrile with 0.1% TFA. For LC-MS characterization of SulfoCy5-peptide conjugates, please see the Supplementary Information.

PMO Peptide Conjugation:

PMO-peptide conjugates were synthesized using Cu(I) catalyzed azide alkyne cycloaddition using CuBr in DMF. Under N_2, a mixture of peptide alkyne (1.1 μmol), PMO azide (0.95 μmol), and copper bromide (0.05 mmol) was dissolved in DMF, vortexed, and allowed to react for 1 hour. The reaction was quenched with the addition of 10 mL of 50 mM Tris (pH 8), and purified by reverse-phase HPLC using a linear gradient from 5-45% B over 20 minutes. Mobile phase A: 100 mM ammonium acetate pH 7.2 in water. Mobile phase B: acetonitrile. For LC-MS characterization of all PMO-peptide conjugates, please see the Supplementary Information.

Flow Cytometry:

HeLa-654 cells were maintained in MEM supplemented with 10% (v/v) fetal bovine serum (FBS) and 1% (v/v) penicillin-streptomycin at 37 °C and 5% CO_2. Eighteen hours prior to treatment, the cells were plated at a density of 5,000 cells per well in a 96-well plate in MEM

supplemented with 10% FBS and 1% penicillin-streptomycin. The day of the experiment, stocks of each PMO-peptide conjugate were prepared in phosphate-buffered saline (PBS) (Note: for experiments with PMO-SulfoCy5-peptide conjugates, the procedure was similar but the stocks were prepared in dimethylsulfoxide – see supporting information for details). The concentration of the stocks was determined by measuring the absorbance at 260 nm and using an extinction coefficient of 168,700 L mol^{-1} cm^{-1}. Cells were incubated with each respective conjugate at a concentration of 5 μM (unless otherwise indicated) in MEM supplemented with 10% FBS and 1% penicillin-streptomycin for 22 hours at 37 °C and 5% CO_2. Next, the treatment media was aspirated, the cells were incubated with Trypsin-EDTA 0.25 % for 15 min at 37 °C and 5% CO_2, washed 1x with PBS, and resuspended in PBS with 2% FBS and 2 μg/mL propidium iodide. The PMO-CPPs in Figure 2A were tested at Sarepta Therapeutics and all remaining experiments were performed at MIT on a BD LSRII flow cytometer using HeLa-654 cells obtained from the University of North Carolina Tissue Culture Core facility. Gates were applied to the data to ensure that cells that were highly positive for propidium iodide or had forward/side scatter readings that were sufficiently different from the main cell population were excluded. Each histogram contains at least 3,000 gated events, with the exception of cells treated with PMO-Melittin-Bpep and several of the 25 μM treatments.

Inhibitor Experiments:

To inhibit a variety of endocytic mechanisms, a pulse-chase experiment was performed. Briefly, HeLa-654 cells were plated at a density of 5,000 cells per well in a 96-well plate in MEM supplemented with 10% FBS and 1% penicillin-streptomycin. The next day, the cells were treated with each inhibitor at the indicated concentration. After 30 minutes, PMO-peptide conjugate was added to each well at a concentration of 5 μM. After incubation at 37 °C and 5%

CO_2 for 3 hours, the treatment media was replaced with fresh media (no inhibitor or PMO-peptide) and the cells were allowed to grow for another 22 hours at 37 °C and 5% CO_2. For the 4 °C experiments, the day after plating, the cells were pre-incubated for 30 minutes at 4 °C, followed by the addition of PMO-peptide conjugate to each well at a concentration of 5 μM. After incubation at 4 °C for 3 hours, the treatment media was replaced with fresh media and the cells were allowed to grow for another 22 hours at 37 °C and 5% CO_2. Sample preparation and flow cytometry was then performed as described above. Each histogram contains at least 3,000 gated events, with the exception of treatment with 20 μM cytochalasin D.

Live-Cell Confocal Imaging:

HeLa-654 cells were plated at a density of 5,000 cells per well in a #1.5 coverslip glass-bottom 96-well plate in MEM supplemented with 10% FBS and 1% penicillin-streptomycin. Twenty-four hours later, PMO-SulfoCy5-peptide conjugate was added to each well at a concentration of 5 μM. Six hours after that (sixteen hours prior to imaging), 3 μL of CellLight™ Early Endosomes-RFP, BacMam 2.0 was added to each well (corresponding to 30 particles per cell). To prepare for imaging, the treatment media was aspirated, the cells were washed twice with PBS, the cells were stained for 10 minutes with 2 μg/mL Hoechst in PBS followed by two more PBS washes. Finally, the cells were imaged in PBS on an RPI spinning disk confocal microscope.

Melting Temperature Analysis:

The melting temperature for dissociation of PMO from its complementary sequence was measured for the unmodified PMO, PMO-pVEC, PMO-Bpep, and PMO-pVEC-Bpep to assess binding. Each construct was incubated with its complementary DNA strand (Integrated DNA Technologies) in PBS for 30 minutes at room temperature (50 μM each, 20 μL total volume). An

intercalating fluorescent dye (EvaGreen, Biotium) was then added and samples were incubated for 30 minutes at room temperature. A melting experiment was performed using a quantitative real-time PCR machine (BioRad CFX96 Real-Time System) by increasing the temperature from 40 °C to 100 °C in 0.5 °C increments. Fluorescence at 520 nm was measured at each increment, with PMO/DNA melting corresponding to a decrease in fluorescence. Melting temperature (T_m) was calculated from three experimental replicates.

Results and Discussion:

Our initial proof-of-concept experiments were aimed at determining if chimeric CPPs could improve PMO efficacy. We designed a set of three constructs that combine an arginine-rich CPP with an amphipathic CPP. Each construct has three components: the two CPPs and the PMO. The two CPPs were linked through an amide bond to generate one long, linear peptide. The C-terminal peptide for each construct was Bpep, an arginine-rich CPP that has consistently been one of the highest performing CPPs for PMO delivery.[9,11,25] For the N-terminal peptide, we chose three known amphipathic CPPs: pVEC, penetratin, and mellitin.[26–28] One additional construct was generated with Bpep as the N-terminal peptide to serve as a standard of comparison in which the chimera consists of two arginine-rich peptides (Figure 1A). The PMO cargo employed was a 6 kDa, 18-base pair PMO that can trigger increased eGFP expression in a HeLa cell line stably transfected with a split eGFP construct (Figure 1B).

To synthesize the constructs, the two-component, chimeric peptide was prepared by automated fast-flow solid-phase peptide synthesis.[24] The N-terminus of the peptide was capped with 4-pentynoic acid to provide a click chemistry handle. The PMO was provided by Sarepta Therapeutics and functionalized at the 3'-amine with 5-azidopentanoic acid. The PMO was

conjugated to the chimeric peptide using copper-catalyzed click chemistry and the PMO-chimera conjugates were purified by reversed-phase high-performance liquid chromatography (RP-HPLC) (Figure 1B).

Next, the conjugates were evaluated in the HeLa-654 eGFP assay to assess if the chimeric CPPs would improve PMO efficacy. In this assay, the HeLa cells are stably transfected with an eGFP sequence that is interrupted with a mutated intron of the human β-globin gene (IVS2-654). The mutation creates a cryptic splice site that leads to retention of a β-globin fragment in the eGFP mRNA sequence. Upon translation, the eGFP is nonfluorescent. The IVS2-654 PMO utilized in the conjugates hybridizes to the mutated intron and prevents the aberrant pre-mRNA splicing, leading to an eGFP mRNA sequence that encodes for functional, fluorescent eGFP. The amount of PMO delivered is therefore correlated to the amount of functional eGFP expressed. However, multiple factors, such as endosomal escape, nuclear localization, and pre-MRNA-splicing activity, will influence the amount of eGFP fluorescence observed after treatment with a given PMO conjugate.

The HeLa-654 cells were treated with 5 μM of each conjugate in serum-containing media. After 22 hours, the fluorescence of the cells was analyzed by flow cytometry (Figure 1C). All four CPP chimeras performed better than Bpep, the consistently high-performing CPP for PMO delivery. Our top chimera, PMO-Penetratin-Bpep, had an approximately 70-fold increase in eGFP fluorescence compared to the background fluorescence of untreated cells. For reference, this is over a 20-fold improvement with respect to the unconjugated PMO and a 2-fold improvement with respect to PMO-Bpep.

Both PMO-Penetratin-Bpep and PMO-pVEC-Bpep displayed synergy, in which the activity of the PMO-chimeric CPP was greater than the sum of the expected activities from each of the

PMO-CPPs individually. For example, PMO-Penetratin demonstrated a 7-fold increase and PMO-Bpep demonstrated a 35-fold increase in eGFP fluorescence. An additive effect would lead to a 42-fold increase in eGFP fluorescence for PMO-Penetratin-Bpep. However, the PMO-Penetratin-Bpep chimera had an almost 70-fold increase in eGFP fluorescence, meaning it performed approximately 1.5 times better than an additive effect. A similar synergy was also observed for PMO-pVEC-Bpep, in which the measured eGFP fluorescence was also 1.5 times greater than the sum of the parts.

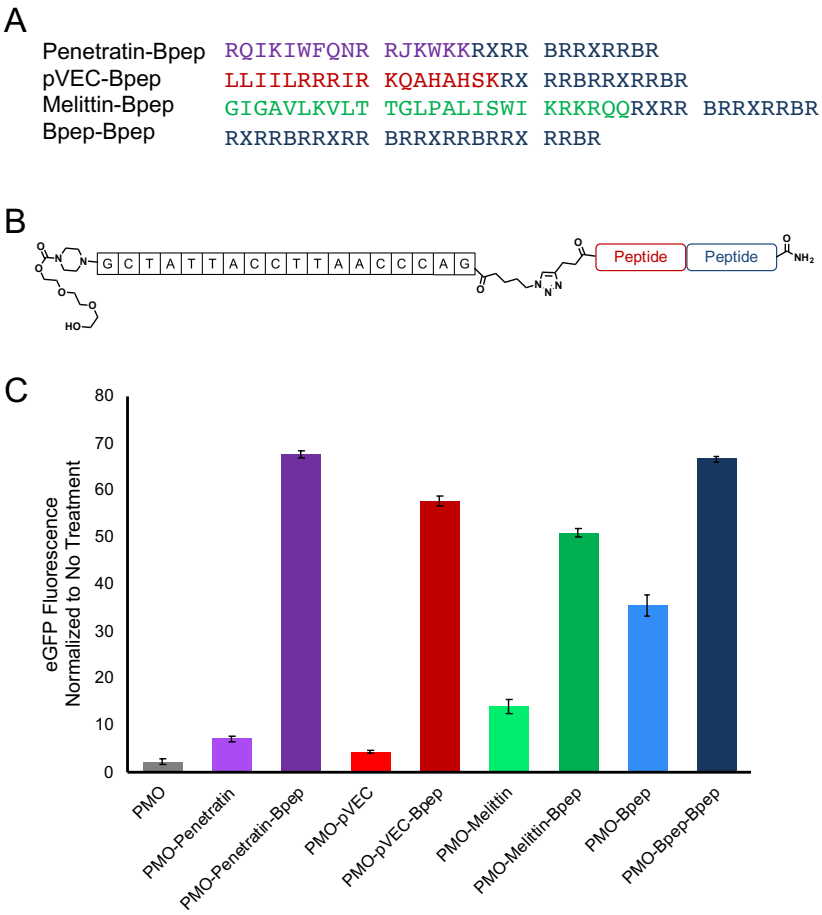

Figure 1: PMO-peptide chimera conjugates enhance exon skipping. A) Amino acid sequences of the four cell-penetrating peptide chimeras used in this work. Each chimera includes

one cell-penetrating peptide on the N-terminus followed by Bpep on the C-terminus. X = aminohexanoic acid, B = beta-alanine and J = norleucine. B) General scheme of a PMO-chimera conjugate. C) Plot showing mean eGFP fluorescence of a population of stably transfected HeLa-654 cells after continuous treatment for 22 hours with 5 μM of each PMO-peptide conjugate. The mean eGFP fluorescence was normalized to the eGFP fluorescence of untreated cells. Both PMO-Penetratin-Bpep and PMO-pVEC-Bpep demonstrated synergistic improvement in activity over the base PMO-peptide conjugates. Error bars are a standard deviation of a technical triplicate and the increased activity of each PMO-chimera conjugate is statistically significant compared to both PMO-CPP and PMO-Bpep. Statistical analyses were performed using a one-way ANOVA and Bonferroni's multiple comparison test ($p \leq 0.0001$ for all groups). Results are a representative example of several independent experiments that included these constructs and conditions (Figure S1, Figure 3).

The existence of a synergistic effect in two of the chimeras supports the notion that combining an arginine-rich CPP with an amphipathic CPP can improve PMO efficacy. However, other variables could be responsible for the observed effects. The order of the individual peptides may influence PMO activity. Therefore, for each construct, we synthesized the peptide sequences with the order reversed where Bpep is at the N-terminus and the other CPP is at the C-terminus. After conjugation to PMO and purification by RP-HPLC, these conjugates were tested in the eGFP assay along with their counterparts that had Bpep on the C-terminus. For both synergistic chimeras (PMO-Penetratin-Bpep and PMO-pVEC-Bpep), switching the order of the peptides decreased observed PMO activity (Figure 2A, Figure S1). This observation suggests that it is critical to have Bpep as the C-terminal component to observe synergy.

This result raises the question of whether or not the N-terminal peptide has functional significance. Alternatively, the N-terminal peptide could serve as a spacer between the PMO and Bpep that amplifies the effect of Bpep. If this were true, it would explain why all four chimeras with Bpep at the C-terminus performed similarly. To address this question, we prepared chimeras in which the N-terminal peptide was replaced by a 15-residue polyproline or polyalanine spacer. The two spacers are of identical length but will likely exhibit different structures given the rigidity of polyproline sequences. PMO-P15-Bpep and PMO-A15-Bpep were evaluated in the eGFP assay (Figure 2B). PMO-P15-Bpep showed no improvement over PMO-Bpep. However, PMO-A15-Bpep exhibited a mean fluorescence intensity greater than PMO-Bpep and performed almost as well as the CPP chimeras. Unfortunately, comparison of this result to PMO-A15 was prevented due to the poor synthesis and solubility of A15, which limits assessment of whether or not the effect is synergistic. P15 and A15 had divergent effects as the N-terminal peptide, indicating that while spacing may play a role in the efficacy of the chimeric CPPs, it likely does not fully account for the effect of the N-terminal peptide in the chimeric sequence.

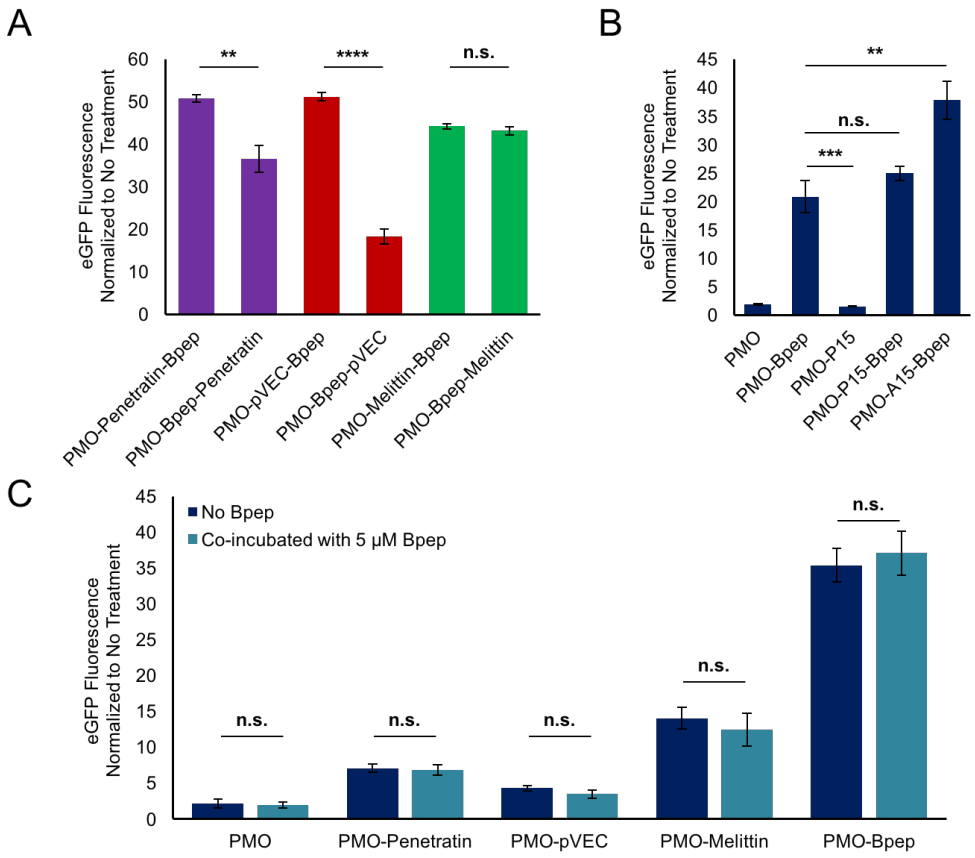

Figure 2: The activity of PMO-CPP chimera conjugates is influenced by specific design features. (A) For each chimera, the order of the sequences was reversed and the activity of the PMO-peptide conjugate was measured in the eGFP assay. The plot shows the fold change in eGFP fluorescence relative to the untreated control. B) Plot of the fold change in eGFP fluorescence for cells treated with 5 µM of PMO, PMO-P15, PMO-Bpep, PMO-P15-Bpep, or PMO-A15-Bpep for 22 hours. C) Comparison of the fold change in eGFP fluorescence for HeLa-654 cells treated with 5 µM of each base PMO-CPP for 22 hours in the presence or absence of 5 µM Bpep. For each construct, the difference in activity with and without B-pep co-incubation was not statistically significant. For every experiment displayed in the figure, error bars represent a standard deviation of a technical triplicate and statistical analyses were performed using a student's t-test (**** $p \leq 0.0001$, *** $p \leq 0.001$, ** $p \leq 0.01$, n.s. $p > 0.05$).

Next, we investigated the necessity of covalent attachment. The increase in PMO activity may or may not require the two component peptides of the chimera to be covalently attached. The eGFP assay was repeated with PMO-Penetratin, PMO-pVEC, PMO-Melittin and PMO-Bpep in either the presence or absence of 5 μM Bpep (Figure 2C). In all cases, the PMO-CPP conjugates performed identically, regardless of whether or not Bpep was present. This result demonstrates that covalently linking the two CPPs is necessary to observe an improvement in activity. Co-incubation with Bpep did not result in any change in eGFP fluorescence.

Given concerns over the size and net charge of the constructs, a lactate dehydrogenase assay was performed to assess if the plasma membrane of the cells had been compromised in any way during treatment with the chimeric constructs (Figure S2). At 5 μM, none of the constructs except for the PMO-Melittin-Bpep construct caused additional lactate dehydrogenase release compared to untreated cells, suggesting the majority of our chimeras do not disrupt the cell membrane.

Since both efficacy and toxicity can be concentration-dependent, we also assessed the extent to which trends in exon skipping activity and toxicity were consistent across a range of concentrations. Concentrations of 0.2 μM, 1 μM, 5 μM, 10μM and 25 μM were used for treatment in the exon skipping assay described above. Non-chimeric CPP-PMO conjugates exhibited minimal activity at low concentrations and a gradual increase in efficacy with increasing dose (Figure 3). The PMO-chimeras exhibited poor efficacy at 0.2 μM but increased dramatically at 1 μM, with the exception of PMO-pVEC-Bpep which did not increase significantly until 5 μM. Efficacy began to plateau at 10 μM, except for PMO-Melittin-Bpep which could not be measured at 10 μM due to severe toxicity. All PMO-chimeras were toxic at

25 μM. An LDH assay confirmed these results, indicating that the PMO-chimera conjugates exhibited 70 to 100% of the maximum possible LDH release at 25 μM, with some causing significant membrane disruption at 10 μM as well (Figure S3). At lower concentrations however, most of the PMO-chimera conjugates did not exhibit cytotoxicity. Taken together, these data indicate that 5 μM is an optimal dosing window for these chimeric CPPs to mediate exon skipping.

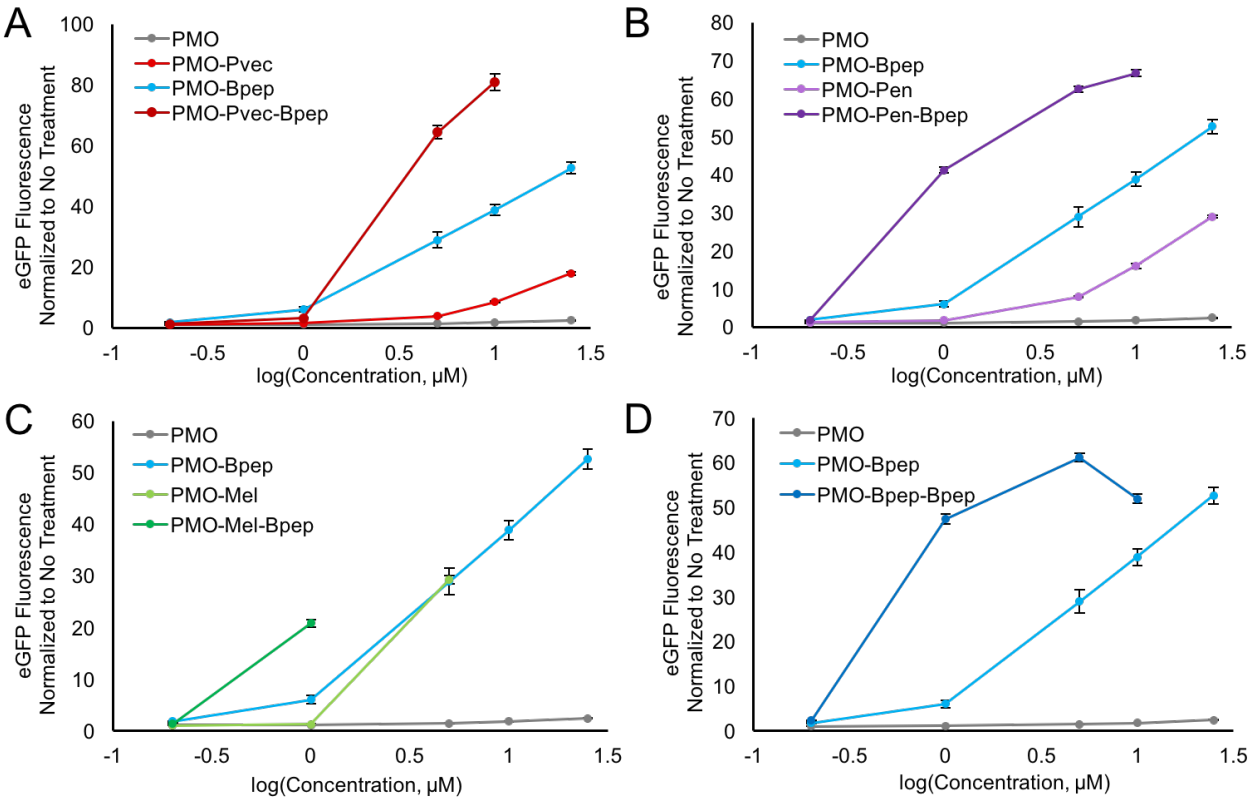

Figure 3: PMO-peptide chimera conjugates exhibit dose dependent activity. For each CPP chimera, HeLa-654 cells were treated with 0.2, 1, 5, 10, and 25 μM of the PMO-chimera, the related PMO-CPPs, and the unmodified PMO. After 22 hours, eGFP fluorescence was measured via flow cytometry. A) PMO-pVEC-Bpep, B) PMO-Penetratin-Bpep, C) PMO-Melittin-Bpep,

D) PMO-Bpep-Bpep. All values are normalized to the eGFP fluorescence of untreated cells. Error bars are a standard deviation of a technical triplicate.

We then probed the mechanism by which these chimeric CPPs improve PMO efficacy. The eGFP HeLa cells provide a functional assay for PMO activity, yet many mechanistic steps contribute to this final read-out. The PMO conjugates must be internalized into cells, escape endosomes if endocytosed, localize to the nucleus, and bind to pre-mRNA to generate an effect. The different parts of the chimera may be aiding in one or many of these steps. While it is challenging to conclusively demonstrate the exact mechanism given the complexity of the biological processes involved, we chose one model chimera to thoroughly study to gain additional insight. PMO-pVEC-Bpep was used for this purpose, since it demonstrated synergy and did not disrupt the plasma membrane at 5 μM. Additionally, the poor performance of PMO-pVEC made the strong performance of PMO-pVEC-Bpep an intriguing result.

Mechanistic studies began with experiments to assess cellular uptake pathways. To examine if energy-dependent pathways are involved, PMO activity was measured after treatment at 4 °C vs. 37 °C. The experiments were performed in a pulse-chase format in which the eGFP HeLa cells were incubated with 5 μM PMO-pVEC, PMO-Bpep, or PMO-pVEC-Bpep for 3 hours at either 4 °C or 37 °C (Figure 4A). Then, the treatment media was exchanged for fresh media and the cells were allowed to grow for an additional 22 hours. For all compounds except PMO-Bpep, there was a decrease in eGFP fluorescence when treated at 4 °C. This result suggests that energy-dependent mechanisms are relevant to the uptake of the PMO-pVEC-Bpep chimera. With respect to the PMO-Bpep result, any conjugate that binds to the surface of the cells during treatment at 4

°C could be subsequently internalized and trigger eGFP expression when the cells are incubated for an additional 22 hours at 37 °C after treatment.

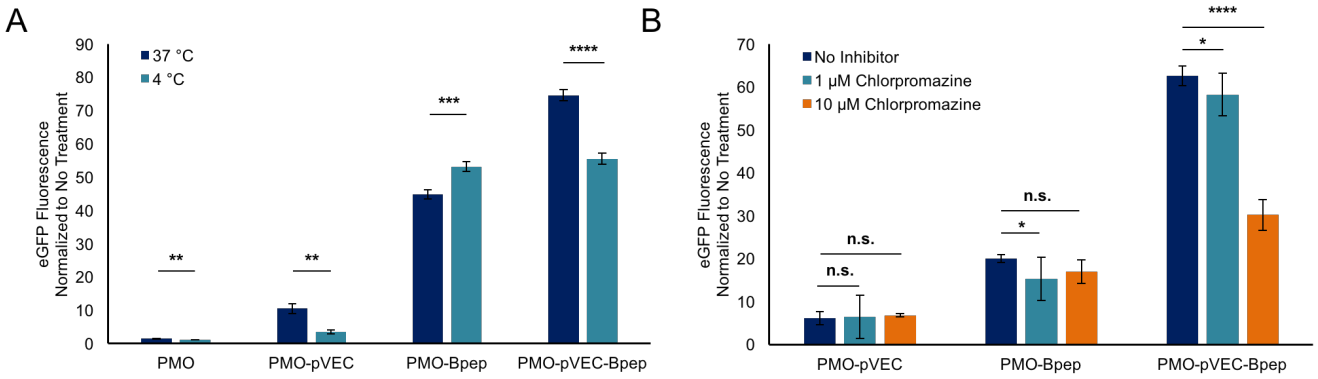

Figure 4: PMO-pVEC-Bpep conjugate undergoes energy-dependent uptake via a route distinct from the PMO-CPPs. A) Plot of normalized eGFP fluorescence for cells treated at either 37 ºC or 4 ºC, normalized to the respective untreated control. The cells were allowed to equilibrate to their respective temperatures for 30 minutes prior to treatment with 5 μM PMO, PMO-pVEC, PMO-Bpep, or PMO-pVEC-Bpep. After treatment with the constructs for 3 hours, the media was exchanged for fresh, untreated media and the cells from both conditions were incubated for another 22 hours at 37 ºC. Both PMO-pVEC and PMO-pVEC-Bpep exhibited a reduction in uptake at 4 ºC, suggesting that energy-dependent processes are relevant for uptake. Statistical analyses were performed using a student's t-test (**** $p \leq 0.0001$, *** $p \leq 0.001$, ** $p \leq 0.01$). B) Plot of normalized eGFP fluorescence for cells treated with different concentrations of chlorpromazine, normalized to the untreated control. The cells were pre-incubated for 30 minutes with chlorpromazine and then 5 μM PMO, PMO-pVEC, PMO-Bpep, or PMO-pVEC-Bpep was added. After treatment with the constructs for 3 hours, the media was exchanged for fresh, untreated media and the cells from both conditions were incubated for another 22 hours at 37 ºC. At 10 μM chlorpromazine, eGFP fluorescence decreased only in the cells treated with the PMO-pVEC-Bpep chimera, suggesting that clathrin-mediated endocytosis plays a unique role in

the uptake of the chimera. Statistical analyses were performed using a one-way ANOVA and Sidak's multiple comparison test (**** $p \leq 0.0001$, * $p \leq 0.05$, n.s. $p > 0.05$). For both experiments, error bars are a standard deviation of a technical triplicate.

In addition, we studied the effect of multiple endocytosis inhibitors on the internalization of PMO-pVEC, PMO-Bpep, and PMO-pVEC-Bpep into cells (Figure 4B, Figure S4). The experiments were performed in a pulse-chase format in which the eGFP HeLa cells were pre-incubated with the inhibitors. After thirty minutes of pre-incubation, the PMO-peptide conjugates were added and after three hours, the treatment media was exchanged with fresh media and the cells were left to grow for another 22 hours. The majority of the inhibitors had no effect. However, at high concentrations of chlorpromazine, eGFP fluorescence decreased in the cells treated with the PMO-pVEC-Bpep chimera. While chlorpromazine is considered an inhibitor of clathrin-mediated endocytosis, it may possibly affect downstream components of the process too.[29] Beyond the possible role of clathrin-mediated endocytosis in the uptake of the chimera, these data demonstrate that the chimera is accessing a unique internalization mechanism since no appreciable decrease was observed with either PMO-pVEC or PMO-Bpep.

Finally, the constructs were labeled with a small molecule organic dye orthogonal to eGFP to allow simultaneous monitoring of the uptake of the compounds and functional exon-skipping activity. Experiments of this format could help deconvolve cellular internalization from PMO efficacy. The compounds were designed with the dye linked to the amino acid directly adjacent to the PMO such that the dye should be reflective of the localization of the PMO even if the peptide undergoes proteolytic degradation. To prepare these compounds, pVEC, Bpep and pVEC-Bpep were synthesized with a cysteine residue on the N-terminus of the sequence and the

terminus was then capped with 4-pentynoic acid as before. After purification by RP-HPLC, the peptides were dissolved in water with equimolar Sulfo-Cyanine5 maleimide and purified again by RP-HPLC. Finally, the SulfoCy5-labeled peptides were all conjugated to the PMO-azide through copper-catalyzed click chemistry and purified by RP-HPLC.

Using the SulfoCy5-labeled constructs, we performed a flow cytometry experiment with the eGFP HeLa cells. The cells were treated with 5 μM of each conjugate in serum-containing media for 22 hours and then analyzed by flow cytometry (Figure 5A). For eGFP fluorescence, the 488 nm excitation laser and 530 nm emission filter were used, and for the SulfoCy5, the 561 nm excitation laser and 695 nm emission filter were used. The separation of channels enabled fluorescence from both fluorophores to be simultaneously recorded. We also treated with unlabeled PMO-pVEC, PMO-Bpep, and PMO-pVEC-Bpep to determine if the fluorophore was perturbing the effect of a given conjugate. In all cases, eGFP fluorescence was slightly decreased with the fluorophore attached suggesting that while the fluorophore may affect the efficacy of the conjugate, it does so uniformly (Figure S5).

In terms of SulfoCy5 fluorescence, PMO-SulfoCy5-Bpep exhibited less fluorescence than PMO-SulfoCy5-pVEC or PMO-SulfoCy5-pVEC-Bpep. However, PMO-SulfoCy5-Bpep had a relatively high ability to facilitate eGFP expression. This result suggests that while the overall cellular uptake of PMO-Bpep is less than PMO-pVEC, Bpep has a beneficial downstream effect. Perhaps improved endosomal escape, nuclear entry, RNA binding, or splice-modification results in the relatively high eGFP fluorescence for PMO-Bpep. On the other hand, PMO-SulfoCy5-pVEC had high SulfoCy5 fluorescence, but poor eGFP expression, which indicates that the compound has good cellular uptake but has limitations elsewhere downstream. The pVEC-Bpep chimera exhibited both the highest eGFP expression and the highest SulfoCy5 fluorescence,

though the SulfoCy5 fluorescence was on a similar scale to pVEC. Therefore, our hypothesis for the basis of the chimera's synergy is that the pVEC component is improving cellular uptake without interfering with the beneficial downstream effects of Bpep.

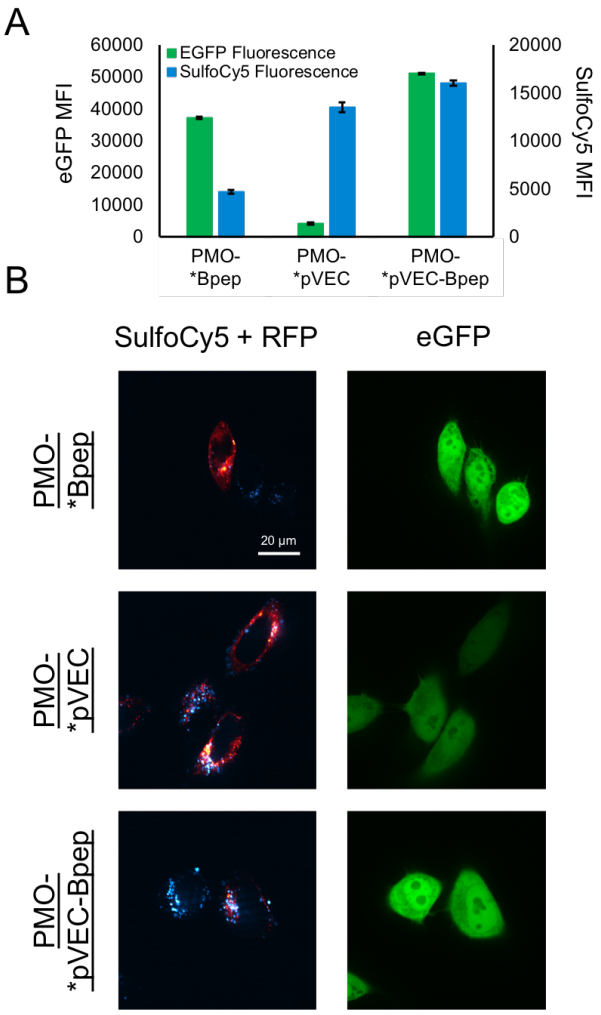

Figure 5: PMO-pVEC-Bpep exhibits high internalization and high exon skipping activity. A) Plot showing the mean fluorescence intensity (MFI) in each respective channel for eGFP and SulfoCy5 for HeLa-654 cells treated with 5 µM PMO-SulfoCy5-pVEC, PMO-SulfoCy5-Bpep, or PMO-SulfoCy5-pVEC-Bpep for 22 hours at 37 ºC. The left axis pertains to eGFP fluorescence and the right axis pertains to SulfoCy5 fluorescence. PMO-*Peptide is a figure

abbreviation for a PMO-SulfoCy5-Peptide construct. Error bars are a standard deviation of a technical triplicate. For both eGFP and SulfoCy5 fluorescence, the activity of PMO-pVEC-Bpep, PMO-pVEC, and PMO-Bpep are all statistically different ($p \leq 0.0001$, analyses performed using a one-way ANOVA and Tukey's multiple comparison test). B) Live-cell confocal microscopy images of HeLa-654 cells after treatment with the same conditions as the flow cytometry experiments. The cells were also transiently transfected with an RFP-Rab5a fusion construct to label early endosomes (green - eGFP - PMO activity, red – RFP – early endosomes, cyan – SulfoCy5 – conjugates). For visualization of nuclei and brightfield images, see Appendix 2 of the supporting information.

To test the hypothesis that the pVEC component improves cellular uptake, we performed live cell confocal microscopy imaging experiments on the eGFP HeLa cells. The same treatment conditions as the flow cytometry assay were used except that a Rab5a-RFP fusion protein was used to label early endosomes and Hoechst dye was used to label nuclei. The eGFP HeLa cells were transiently transfected sixteen hours prior to imaging with a Rab5a-RFP fusion construct in order to examine the extent of localization to endosomes. We reasoned that if PMO-SulfoCy5-pVEC had poor efficacy in triggering eGFP expression due to endosomal entrapment, the RFP signal would be co-localized with the SulfoCy5 signal. In addition, labeling with Hoechst dye enabled the nuclear regions to be delineated and the nuclear SulfoCy5 signal to be quantified.

The imaging data correlate well with the flow cytometry data (Figure 5B). With both PMO-SulfoCy5-pVEC and PMO-SulfoCy5-pVEC-Bpep, the bright SulfoCy5 signal is mostly concentrated in punctae. Some SulfoCy5 signal is co-localized with RFP signal, with Mander's Colocalization Coefficients of 0.4 ± 0.1 and for PMO-SulfyCy5-pVEC and PMO-SulfoCy5-

pVEC-Bpep, respectively (see Section 8 of SI for details). This indicates that approximately 40% of the SulfoCy5-labeled construct is co-localized with RFP, suggesting localization to the early endosome. Other SulfoCy5 punctae are likely late endosomes and lysosomes. These images provide further evidence that the primary mechanism of internalization is endocytosis and that endosomal entrapment can limit PMO activity for certain constructs, despite significant cellular uptake.

With regard to the nuclear SulfoCy5 signal, PMO-SulfoCy5-pVEC-Bpep exhibited the highest mean nuclear fluorescence (Figure S6). The nuclear fluorescence was determined by labeling the nuclei with Hoechst, outlining the nuclear regions, and quantifying SulfoCy5 signal in the nuclear regions. Intriguingly, the nuclear SulfoCy5 fluorescence of PMO-SulfoCy5-pVEC was higher than PMO-SulfoCy5-Bpep, even though PMO-SulfoCy5-Bpep exhibited more eGFP signal. Because multiple factors influence the amount of eGFP fluorescence observed after treating the HeLa-654 cells, the higher activity combined with a lower nuclear concentration suggests that the Bpep component may lead to enhanced splicing activity independent of delivery.

We then analyzed the impact of peptide conjugation on PMO binding to its complementary oligonucleotide sequence. Although the PMO exerts exon skipping activity by binding pre-mRNA, we considered single-stranded DNA to be a good proxy for comparing the relative binding affinity of these PMO-peptide conjugates *in vitro*, given that relative trends in antisense oligonucleotide binding affinity are generally conserved between RNA and DNA.[30,31] We obtained melting curves for the unmodified PMO, PMO-Bpep, PMO-pVEC, and PMO-pVEC-Bpep each combined with DNA sequence complementary to the PMO (Figure 6A, Figure S7). We then determined the melting temperature (T_m) for each construct from the derivative of the

corresponding melting curve, where the maximum of this derivative plot corresponds to the T_m (Figure 6B, Figure S7).

A

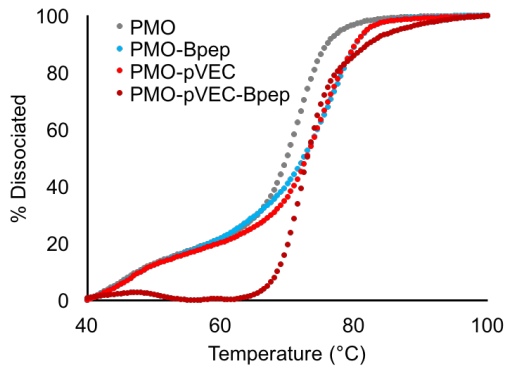

B

	T_m (°C)
PMO	71.3 ± 0.3
PMO-Bpep	77.3 ± 0.3
PMO-pVEC	75 ± 3
PMO-pVEC-Bpep	72.3 ± 0.6

Figure 6. Peptide conjugation slightly alters PMO binding to a complementary nucleic acid. A) Melting curves for the unmodified PMO, PMO-Bpep, PMO-pVEC, and PMO-pVEC-Bpep annealed to the complementary DNA sequence. Melting was monitored via fluorescence decrease of an intercalating dye. Fluorescence measurements were then normalized and converted to percent dissociated. Shown is one representative independent experiment of three total independent experiments, with remaining replicates shown in Figure S7. B) The T_m for each construct was calculated from the derivative of the corresponding melting curve. Values represent the average of three independent experiments with an error of one standard deviation.

The melting curves as well as the T_m values indicate that peptide conjugation slightly enhances PMO affinity for its target sequence, with a maximum increase in T_m of (6.0 ± 0.4) °C for PMO-

Bpep. It is possible that this slight increase in binding affinity could contribute to the increase in exon skipping activity noted for PMO-Bpep despite its lower observed nuclear localization. However, the differences in T_m between the three PMO-peptide conjugates was relatively low, indicating that peptide identity does not have a dramatic impact on the affinity of the PMO for its complementary sequence. Further, PMO-pVEC-Bpep exhibited the smallest increase in T_m relative to the unmodified PMO. Altogether, this suggests that the mechanism by which the pVEC-Bpep chimera enhances exon skipping is not related to improved PMO binding to its target sequence.

Further experiments will be necessary to precisely define the effects downstream of internalization that are involved in the synergistic performance of the chimeras. However, here we show with our mechanistic studies that individual CPPs may be helpful with different elements of macromolecule delivery. We show that chimeric peptides composed of CPPs can exhibit synergistic improvements in PMO delivery and exon skipping efficiency. We show that the relative position of the sequences affects the degree of uptake, that peptide identity tunes activity, and that they must be covalently attached to observe the effect. One issue with this strategy is the large molecular weight of the resultant conjugates. One way to overcome this would be to create deletion analogues to identify the minimal necessary sequence to observe synergy. These deletion constructs will be the subject of future investigations with the Penetratin-Bpep and pVEC-Bpep chimeras.

Given that poor intracellular delivery has largely limited the therapeutic application of antisense oligonucleotides, we believe this strategy could help improve conjugate therapies for the treatment of several genetic diseases, such as Duchenne muscular dystrophy. More generally,

we envision that the approach of combining CPPs from different classes can be applied to the intracellular delivery of a variety of macromolecular cargoes.

ASSOCIATED CONTENT

Supporting Information:

Methods for peptide synthesis and conjugation, lactate dehydrogenase assay results, flow cytometry analysis of PMO-chimeras in the presence of endocytosis inhibitors, LC-MS analysis of peptide conjugates, flow cytometry analysis of fluorophore-labeled PMO-chimeras, and co-localization analysis and nuclear fluorescence quantification of confocal images.

AUTHOR INFORMATION

Corresponding Author:

* E-mail: blp@mit.edu

Author Contributions:

† C.M.F., R.L.H., and J.M.W. contributed equally to this work.

Funding Sources:

This work was supported by Sarepta Therapeutics, Cambridge MA. J.M.W. and R.L.H are supported by the National Science Foundation Graduate Research Fellowship under Grant No. 1122374. C.M.F. is supported by the David H. Koch Graduate Fellowship Fund and by the Eunice Kennedy Shriver National Institute of Child Health and Human Development of the National Institutes of Health under award number F30HD093358.

Notes:

The authors declare the following competing financial interest(s): GJH and MY are employees of Sarepta Therapeutics.

ACKNOWLEDGEMENTS

The authors acknowledge the Swanson Biotechnology Center Flow Cytometry Facility at the Koch Institute for advice and the use of their flow cytometers. The authors also acknowledge Wendy Salmon and the W.M. Keck Biological Imaging Facility at the Whitehead Institute for advice and the use of their confocal microscope. We thank Dr. Daniel Chinnapen for his advice on image analysis. We thank Christine Isabella and Prof. Laura Kiessling for assistance with the melting temperature experiments and use of their qPCR instrument. We thank Dr. Ethan Evans and Dr. Alan Beggs for helpful discussions.

REFERENCES

(1) Lim, K. R. Q., Maruyama, R., and Yokota, T. (2017) Eteplirsen in the treatment of Duchenne muscular dystrophy. *Drug Des Devel Ther 11*, 533–545.
(2) Summerton, J., and Weller, D. (1997) Morpholino Antisense Oligomers: Design, Preparation, and Properties. *Antisense and Nucleic Acid Drug Development 7*, 187–195.
(3) Youngblood, D. S., Hatlevig, S. A., Hassinger, J. N., Iversen, P. L., and Moulton, H. M. (2007) Stability of Cell-Penetrating Peptide–Morpholino Oligomer Conjugates in Human Serum and in Cells. *Bioconjugate Chem. 18*, 50–60.
(4) Hudziak, R. M., Barofsky, E., Barofsky, D. F., Weller, D. L., Huang, S.-B., and Weller, D. D. (1996) Resistance of Morpholino Phosphorodiamidate Oligomers to Enzymatic Degradation. *Antisense and Nucleic Acid Drug Development 6*, 267–272.
(5) Chan, J. H., Lim, S., and Wong, W. F. (2006) Antisense Oligonucleotides: From Design to Therapeutic Application. *Clinical and Experimental Pharmacology and Physiology 33*, 533–540.
(6) Hammond, S. M., Hazell, G., Shabanpoor, F., Saleh, A. F., Bowerman, M., Sleigh, J. N., Meijboom, K. E., Zhou, H., Muntoni, F., Talbot, K., Gait, M. J., and Wood, M. J. A. (2016) Systemic peptide-mediated oligonucleotide therapy improves long-term survival in spinal muscular atrophy. *Proc. Natl. Acad. Sci. U.S.A. 113*, 10962–10967.

(7) Betts, C., Saleh, A. F., Arzumanov, A. A., Hammond, S. M., Godfrey, C., Coursindel, T., Gait, M. J., and Wood, M. J. (2012) Pip6-PMO, A New Generation of Peptide-oligonucleotide Conjugates With Improved Cardiac Exon Skipping Activity for DMD Treatment. *Mol Ther Nucleic Acids 1*, e38.
(8) Moulton, H. M., Nelson, M. H., Hatlevig, S. A., Reddy, M. T., and Iversen, P. L. (2004) Cellular Uptake of Antisense Morpholino Oligomers Conjugated to Arginine-Rich Peptides. *Bioconjugate Chem. 15*, 290–299.
(9) Wu, R. P., Youngblood, D. S., Hassinger, J. N., Lovejoy, C. E., Nelson, M. H., Iversen, P. L., and Moulton, H. M. (2007) Cell-penetrating peptides as transporters for morpholino oligomers: effects of amino acid composition on intracellular delivery and cytotoxicity. *Nucleic Acids Res 35*, 5182–5191.
(10) Moulton, H. M., and Moulton, J. D. (2010) Morpholinos and their peptide conjugates: Therapeutic promise and challenge for Duchenne muscular dystrophy. *Biochimica et Biophysica Acta (BBA) - Biomembranes 1798*, 2296–2303.
(11) Wu, B., Moulton, H. M., Iversen, P. L., Jiang, J., Li, J., Li, J., Spurney, C. F., Sali, A., Guerron, A. D., Nagaraju, K., Doran, T., Lu, P., Xiao, X., and Lu, Q. L. (2008) Effective rescue of dystrophin improves cardiac function in dystrophin-deficient mice by a modified morpholino oligomer. *PNAS 105*, 14814–14819.
(12) Langel, Ü. (Ed.). (2011) Cell-Penetrating Peptides. Humana Press, Totowa, NJ.
(13) Copolovici, D. M., Langel, K., Eriste, E., and Langel, Ü. (2014) Cell-Penetrating Peptides: Design, Synthesis, and Applications. *ACS Nano 8*, 1972–1994.
(14) Eiríksdóttir, E., Konate, K., Langel, Ü., Divita, G., and Deshayes, S. (2010) Secondary structure of cell-penetrating peptides controls membrane interaction and insertion. *Biochimica et Biophysica Acta (BBA) - Biomembranes 1798*, 1119–1128.
(15) Thorén, P. E. G., Persson, D., Esbjörner, E. K., Goksör, M., Lincoln, P., and Nordén, B. (2004) Membrane Binding and Translocation of Cell-Penetrating Peptides. *Biochemistry 43*, 3471–3489.
(16) Lundin, P., Johansson, H., Guterstam, P., Holm, T., Hansen, M., Langel, Ü., and EL Andaloussi, S. (2008) Distinct Uptake Routes of Cell-Penetrating Peptide Conjugates. *Bioconjugate Chem. 19*, 2535–2542.
(17) Kosuge, M., Takeuchi, T., Nakase, I., Jones, A. T., and Futaki, S. (2008) Cellular Internalization and Distribution of Arginine-Rich Peptides as a Function of Extracellular Peptide Concentration, Serum, and Plasma Membrane Associated Proteoglycans. *Bioconjugate Chem. 19*, 656–664.
(18) Tünnemann, G., Martin, R. M., Haupt, S., Patsch, C., Edenhofer, F., and Cardoso, M. C. (2006) Cargo-dependent mode of uptake and bioavailability of TAT-containing proteins and peptides in living cells. *FASEB J 20*, 1775–1784.
(19) Madani, F., Lindberg, S., Langel, Ü., Futaki, S., and Gräslund, A. (2011) Mechanisms of Cellular Uptake of Cell-Penetrating Peptides. *Journal of Biophysics*. Research article.
(20) Duchardt, F., Fotin-Mleczek, M., Schwarz, H., Fischer, R., and Brock, R. (2007) A Comprehensive Model for the Cellular Uptake of Cationic Cell-penetrating Peptides. *Traffic 8*, 848–866.
(21) Mayor, S., and Pagano, R. E. (2007) Pathways of clathrin-independent endocytosis. *Nature Reviews Molecular Cell Biology 8*, 603.
(22) Yin, H., Boisguerin, P., Moulton, H. M., Betts, C., Seow, Y., Boutilier, J., Wang, Q., Walsh, A., Lebleu, B., and Wood, M. J. (2013) Context Dependent Effects of Chimeric Peptide

Morpholino Conjugates Contribute to Dystrophin Exon-skipping Efficiency. *Mol Ther Nucleic Acids 2*, e124.
(23) Abes, S., Turner, J. J., Ivanova, G. D., Owen, D., Williams, D., Arzumanov, A., Clair, P., Gait, M. J., and Lebleu, B. (2007) Efficient splicing correction by PNA conjugation to an R6-Penetratin delivery peptide. *Nucleic Acids Res 35*, 4495–4502.
(24) Mijalis, A. J., Thomas Iii, D. A., Simon, M. D., Adamo, A., Beaumont, R., Jensen, K. F., and Pentelute, B. L. (2017) A fully automated flow-based approach for accelerated peptide synthesis. *Nat Chem Biol 13*, 464–466.
(25) Yin, H., Moulton, H. M., Seow, Y., Boyd, C., Boutilier, J., Iverson, P., and Wood, M. J. A. (2008) Cell-penetrating peptide-conjugated antisense oligonucleotides restore systemic muscle and cardiac dystrophin expression and function. *Hum Mol Genet 17*, 3909–3918.
(26) Elmquist, A., Lindgren, M., Bartfai, T., and Langel U, null. (2001) VE-cadherin-derived cell-penetrating peptide, pVEC, with carrier functions. *Exp. Cell Res. 269*, 237–244.
(27) Derossi, D., Joliot, A. H., Chassaing, G., and Prochiantz, A. (1994) The third helix of the Antennapedia homeodomain translocates through biological membranes. *J. Biol. Chem. 269*, 10444–10450.
(28) Terwilliger, T. C., and Eisenberg, D. (1982) The structure of melittin. II. Interpretation of the structure. *J. Biol. Chem. 257*, 6016–6022.
(29) Dutta, D., and Donaldson, J. G. (2012) Search for inhibitors of endocytosis. *Cell Logist 2*, 203–208.
(30) Gryaznov, S. M., Lloyd, D. H., Chen, J. K., Schultz, R. G., DeDionisio, L. A., Ratmeyer, L., and Wilson, W. D. (1995) Oligonucleotide N3'-->P5' phosphoramidates. *PNAS 92*, 5798–5802.
(31) Jensen, K. K., Orum, H., Nielsen, P. E., and Nordén, B. (1997) Kinetics for hybridization of peptide nucleic acids (PNA) with DNA and RNA studied with the BIAcore technique. *Biochemistry 36*, 5072–5077.